Materials Research. 2024; 27:e20240020
DOI: https://doi.org/10.1590/1980-5373-MR-2024-0020

Porous Density Influence on Anti-Corrosive Epoxy Resin-Based Coat Reinforced with Reduced Graphene Oxide (rGO)

***Ananias A. Emmerick*[a*], *Mário N. Barbosa Junior*[a], *Nathália Toste da Silva*[a],**

***João Arthur F. L. Batalha*[b], *I. S. Bott*[a]**

[a]*Pontificia Universidade Católica do Rio de Janeiro (PUC-Rio), Departamento de Engenharia de Materiais e Química, 22453-900, Rio de Janeiro, RJ, Brasil.*
[b]*Universidade Federal do Rio de Janeiro (UFRJ), Instituto de Macromoléculas Professora Eloisa Mano (IMA), 21941-598, Rio de Janeiro, RJ, Brasil.*

Received: January 16, 2024; Revised: May 11, 2024; Accepted: June 16, 2024

The corrosion resistance of an epoxy resin-based coat, reinforced with 0.1 and 0.5 wt% of reduced graphene oxide (rGO), applied to AISI 1020 carbon steel was subjected to immersion tests on a 3.0 wt% NaCl solution saturated with CO_2 in a pressurized cell with 70 bar at 40 °C for 528 hours. The coating was accessed via pull-off testing, and scanning electron microscopy (SEM) was used to analyze porosity and thickness. Optical Microscopy (OM) assessed the condition of the metallic surface. Adding rGO generated greater corrosion protection and improved the structural integrity of the coating for the conditions studied. With 0.1 wt% rGO, there was a pore refinement, and with 0.5 wt%, pore density was drastically reduced. The addition of rGO did not influence the coating Shore D hardness coating. Post-corrosion test results indicated that porosity and solution permeation were related, and the anchorage of the coating to the substrate was not affected.

Keywords: *CO_2 Corrosion, Reduced Graphene Oxide, Pore Refining, Nanocomposite, Novolac Epoxy Resin.*

1. Introduction

The protection of metals and alloys is a widely studied topic[1-4] and is very important for all industry sectors[5]. The coating method is the most used among the anticorrosive methods applied in industrial processes[6,7].

Polymers are the most commonly used in anticorrosive coatings because they have satisfactory thermal stability, humidity resistance, and good anti-corrosion properties[2,8,9]. However, polymeric coatings, when used in environments containing chloride ions[5] or in CO_2, don't prevent moisture penetration, allowing corrosion to occur on the metallic substrate[10].

Consequently, polymer-based microcomposites were developed, such as epoxy paints with glass flakes[11] and monolithic composites, which emerged as an alternative to overcome the limitations of conventional polymeric coatings (additives with filler and /or pigments). Microcomposites demonstrate better resistance to wear, oxidation at elevated temperatures, and corrosion resistance[12,13], even in severe corrosion environments. However, polymer-based microcomposites still have significant limitations when used for a long time, having their lifespan reduced when exposed to natural weathering such as salts, rain, wind, high temperatures, and ultraviolet rays, which can cause loss of color and shine in addition to thickness reduction due to the wear of the polymeric base[14-17]. Two other significant negative characteristics this type of coating presents are the amount and size of pores and micro-cracks. In the long term, these characteristics will offer low resistance to water penetration or corrosive solutions at the metal/coating interface[18,19]. On the other hand, nanocomposites have appeared as an alternative to overcome existing micro and monolithic composites' limitations. Several elements have been used as nanofillers to form nanocomposites with superior anticorrosive properties to conventional coatings and microcomposites. The addition of montmorillonite clay in a polymeric base forms an organic nanocomposite[20], the addition of TiO_2 resin nanofillers in epoxy-based resin[19], the incorporation of ZnO nanoparticles in a melamine-alkyd resin base[21] and the addition of Si nanoparticles in epoxy based resin[22], Fe_2O_3, Al[23,24], $Zn_3(PO_4)_2$, Zn_2SiO, and various mineral fillers such as quartz[14], are some examples. Zhou et al.[25] studied the corrosion resistance of coatings by adding percentages of 1.0, 3.0, and 5.0 wt% of montmorillonite clay (Mnt) nanoparticles in epoxy resin. A metallic substrate was painted and immersed in a solution of 3.0 wt% NaCl for 20 and 120 days, not being informed of the temperature and pressure of the tests. he percentage of 1.0 wt% of Mnt showed the lowest porosity, indicating better barrier properties to the electrolyte when compared to those without Mnt and with 3.0 and 5.0 wt% of Mnt. They obtained positive results regarding the inhibition of penetration of H_2O, O_2, and CO_2, where these corrosive agents showed less development of defects, such as microvoids, bubbles, and cracks in the coating, which damage the

*e-mail: premmerick@gmail.com

physical-chemical and mechanical properties of the system. On the other hand, a study by Rzaij et al.[26] presented the anticorrosive performance of a composite coating formed by epoxy resin with additives with 0.1, 0.3, and 0.5 wt% of nanoparticles of SiO_2. The coated carbon steel substrates were immersed in a solution containing 3.5 wt% NaCl and 5.0% by volume of H_2SO_4, subjected to a temperature of 25 ˚C and a pressure of 1 atmosphere. The results revealed that the anticorrosive action of the coating consisted of epoxy-nano SiO_2 expanded with increasing concentrations of nanosilica. The results also showed a low corrosion rate of 2.51 x 10^{-4} mm/year. The corrosion protection efficiency was approximately 99.77%, and the corrosion rate reduction was 63 times when compared to a substrate coated only with epoxy resin. Additionally, Xu et al.[27] analyzed the anticorrosive coatings composed of water-base epoxy resin immersed in a 10 wt% NaCl solution saturated with CO_2 at 25 °C and atmospheric pressure for 96 hours. The results showed that the water absorption by the epoxy-graphene coating decreased significantly with the increase in graphene addition.

The composite prevented the diffusion of water, providing durable and adequate corrosion protection to the metallic substrate. The epoxy-graphene coating with 0.25 wt% of graphene provided an efficiency of 99.96% compared to the coating without nanoparticle addition. Zhu et al.[28] studied the anticorrosive efficiency of a composite coating made of epoxy resin containing additions of 0.2, 0.5, 0.7, and 1.0 wt% of graphene oxide (GO). N80 steel metallic substrates protected with these composites were immersed in a solution of 3.5 wt% NaCl with a total pressure of 20 MPa and a partial pressure of CO_2 of 5 MPa at 120 ˚C for 60, 120, and 240 hours. The coating containing 0.7 wt% of graphene oxide (GO) was the best evaluated for corrosion resistance due to maximized impermeability and inhibiting the electrolyte's percolation through the coat. The corrosion resistance of the coating with 0.7 wt% of GO was improved by 89.3% compared to the coating without graphene. Therefore, epoxy-graphene-based nanocomposites stand out in more recent anticorrosion applications, demanding more studies in more severe conditions and long-term tests.

A study by Sun et al.[29] on a composite epoxy novolac (EN) system about the influence of water on the high-pressure carbon dioxide resistance of composite coatings indicated that high-pressure CO_2 gas can penetrate the substrate surface through pores of the resin. Therefore, CO_2 diffusion occurs along the interconnection of the pores. They suggested that a suitable volume fraction of particle addition can optimize the pore structure and inhibit the penetration of corrosive ions.

Previous studies reported corrosion tests in a saline-only or saline environment with CO_2 performed at a pressure of only 1 atmosphere and 25 ˚C (room temperature)[28,30-36]. This work aimed to evaluate the corrosion resistance of a composite coating formed by adding percentages of rGO nanoparticles in a polymer-based matrix immersed in a saline environment, saturated with CO_2 at 41 °C and a pressure of 70 bar. The objective is to obtain an anticorrosive coating that presents high efficiency, overcoming the properties of the additive coatings with microcomposites and monolithic composites and avoiding the limitations presented by them.

2. Experimental Section/Methods

2.1. Nanocomposites fabrication and properties

The polymer coating deposited on the metal substrate was an epoxy of commercial origin. The resin was provided without solids, i.e., no fillers or pigments. This commercial epoxy was formed by component A, which consisted of bisphenol F with 1,3-benzenedimethanamine and phenol-formaldehyde and component B, which consisted of a polyamine-based curing agent. The graphene used in this work was chemically synthesized by oxidation and reduction of the commercial graphite Micrograf 99503UJ. Graphite oxide was obtained by chemical exfoliation of graphite using the method employed by Hummers, using 2.3 g of graphite, 2.5 g of $NaNO_4$, 115 mL of H_2SO_4 (98%), 15 g of $KMnO_4$ and 110 mL of H_2O_2 (50%)[10]. Graphene reduction was achieved by the direct action of ultraviolet radiation (OSRAM-Ultravitalux 300W lamp) for 5 hours indoors, resulting in a liquid and reduced graphene oxide sample (called in this work as rOGL). Graphene characterization data has been published elsewhere[10].

The composites were synthesized by adding component B to component A in a proportion of 1:5 in volume, respectively. For example, if the volume of component A is 10 mL, the proportional volume of component B should be 2 mL. The neat epoxy sample was identified as COAT. Also, two more conditions were studied in this work by adding rOGL to a neat epoxy matrix. The contents of graphene were 0.1 and 0.5 wt.%, and the samples were classified as COAT0.1OGL and COAT0.5OGL, respectively. AISI 1020 steel was used as a metallic substrate to measure the coating efficiency in the corrosion tests. AISI 1020 steel was chosen because it is not only low-alloy carbon steel but also available in significant volumes and commonly used to manufacture various items for the industrial area. This steel meets the usual mechanical, structural, and cost requirements. However, it has low performance in terms of corrosion. The standard chemical composition of AISI 1020 steel is shown in Table 1.

The metallic coupons were machined from a drawn flat bar with dimensions of 15 mm in length, 40 mm in width, and 3 mm in thickness (Figure 1).

2.2. Preparation of saline solution for corrosion tests

A saline solution of 3 wt% NaCl was prepared in 1000 mL of distilled water and controlled with 0.4 mL of hydrochloric

Table 1. Chemical composition of the 1020 steel used for the experiments (wt%).

C	Mn	$P_{máx.}$	$S_{máx.}$	F_e
0.18 – 0.23	0.30 – 0.60	0.04	0.05	Bal.

acid to reach pH 5. Next, it was unaired within the vessels by bubbling with nitrogen for 1 hour and saturated for 2 hours with CO_2 bubbled into the solution.

2.3. CO_2 corrosion test

The CO_2 corrosion tests were carried out in a closed system, as shown in Figure 2. This system has two gas lines, N_2 and CO_2, made of stainless steel. The pressure vessels were manufactured in AISI 316L steel, meeting a maximum design pressure of 200 bar. For the corrosion test, 2L of a saline solution with a concentration with a concentration of 3 wt.% NaCl was prepared and placed inside the pressure vessels with a unit volume of 910 mL. All pressure vessels were solution-filled to completion, and the pressure within the vessels was kept at 70 bar throughout the test. For each test condition, three coated samples: COAT, COAT0.1OGL, and COAT0.5OGL, were placed inside these vessels. The coated coupons were arranged on a rod. The arrangement was installed inside each pressure vessel, closed, and the entire system was unaired, including the saline solution (Figure 2).

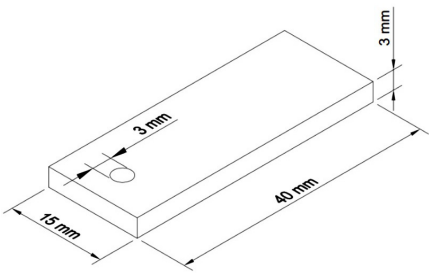

Figure 1. Representative draw of AISI 1020 steel coupons.

Next, the pressure vessels were placed inside a thermostatic bath (Figure 3), set at 41 °C.

After 5 hours, thermal equilibrium was obtained between the thermostatic bath and the saline solution. At the end of the 528 hours test, the thermostatic bath was turned off, and the system was gradually depressurized and opened. The removed coated coupons were immediately dried by hot air and placed in a vacuum desiccator.

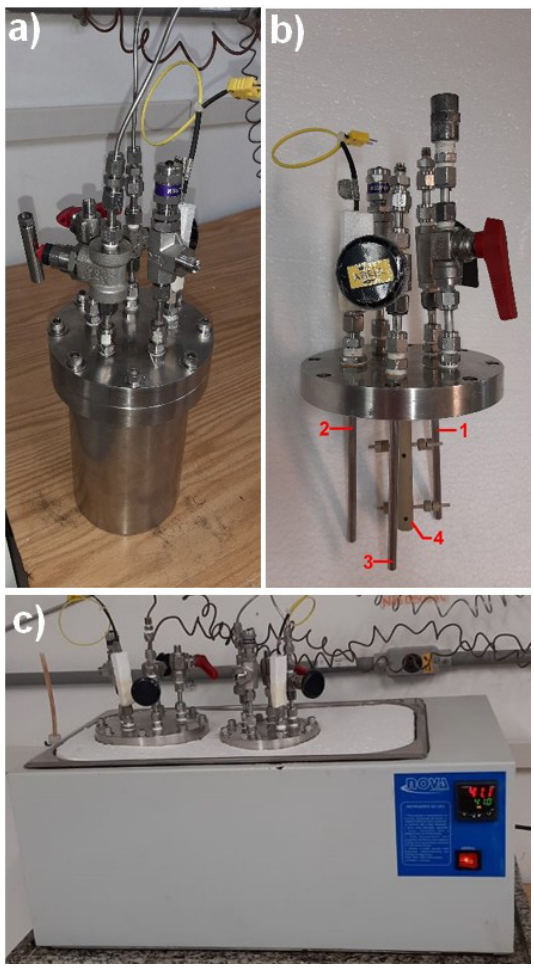

Figure 2. (a) Stainless steel pressure vessel containing saline solution with a concentration of 3 wt% of NaCl, (b) Internal arrangement of pressure vessel lid: (1) CO_2 input, (2) N_2 input, (3) Well to thermocouple, (4) Rod in peek support of coupons and (c) Thermostatic bath with display at 41 °C and pressure vessels connected to the CO_2 and N_2 injection system.

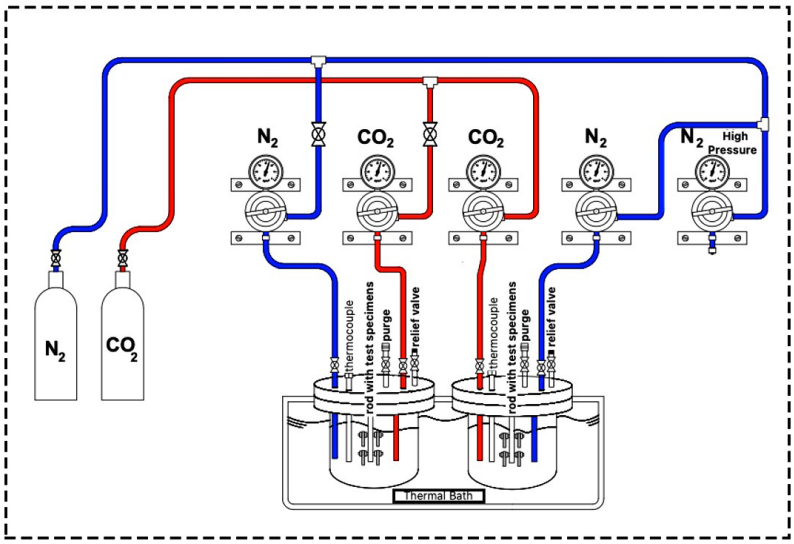

Figure 3. Schematic drawing of the N_2 and CO_2 lines and layout of the connection arrangements in the pressure vessels used for the corrosion tests.

The coating/metal substrate anchorage appearance was characterized using SEM, Cambridge Instruments brand, model: CamScan 3200LV, SEI 20.00 kV, Mag: 1000 x WD scale: 20 µm.

The adhesion resistance (pull-off test) was carried out following ASTM D4541-17[37]. In this test, an anchoring pin (dolly) is placed perpendicular to the coating surface using glue, followed by an applied force to the adhered pin until detachment. The nature of the failure is qualified based on the percentage of adhesive or cohesive failures in the interfaces and layers involved, according to the standard classification.

3. Results and Discussion

3.1. Adherence, bubbles formation and resin pores density

Roughness is essential for the performance and lifespan of coatings applied to a metallic surface[38,39]. Roughness and surface cleanliness are crucial since the adhesion quality of a coating occurs through three bond types: physical, chemical, or mechanical bonds[40]. Physical and chemical bonds can occur due to molecular groups in the resin's chemical structures. These groups will interact with reactive elements or sites on the metallic surface. The samples used in this work follow the technical standards of Petrobras N-2913 Rev.B[41] and Petrobras N-9[42]. According to the obtained images (Figure 4), it is possible to observe that the graphene addition did not interfere with the adhesion properties of the coating. Adhesion to the metallic substrate can be expressed by a satisfactory rupture tension, with an average value of 7.36 MPa in the Pull-Off test for the studied conditions and the coupon's dimensions. Regardless of the purpose of the coating, it is essential to maintain the anchorage integrity of the system (coating/metallic substrate). It was observed that there was good anchoring by the resin to the substrate (Figure 4). The images have been pre-processed and enhanced with ImageJ Version 1.51p software. For COAT, COAT0.1OGL, and COAT0.5OGL, the coating covers the substrate surface even on irregularities resulting from grinding.

The coating acts as a physical barrier between the substrate and the environment. Therefore, impermeability is a fundamental characteristic. When bubbles are formed within the coating, its impermeability is reduced, and consequently, anticorrosive function. Also, there is a possibility of failure concerning the adhesion between the coating and substrate[17]. Air bubbles may also have their origin during the mechanical agitation of the resin/catalyst mixture when these air bubbles are trapped due to the viscosity of the coating[43]. The manufacturer's resin manual used in this study informs that after the addition of the addition of the cure agent during the mix procedures, there will be a tendency to form small bubbles on the surface layer of the resin. The appearance of bubbles and/or pores can be due to the high viscosity and thixotropy of the product[16], inadequate solvent addition, speedy catalyst evaporation, temperature, and air encapsulation. Some or all of these listed causes can occur during mixing and preparation or even during the fast drying of the surface coating. Solvents are volatile organic compounds that solubilize the resins, and it is necessary to impart viscosity to the coating. However, it can cause the inception of bubbles and/or pores that turn out to be points of fragility, which may cause early failure of the coating after evaporation[17]. The curing process in the polymer matrix causes shrinkage of the applied layer of coating, usually around 3-5%, leading to cohesion in the material and fewer pores formed[44-47] since particle addition as fillers interferes with this process. In the present case, the filler is a non-modified graphene oxide particle. It features minimal compatibility with the polymer matrix, and the particles tend to segregate within the matrix. Consequently, it generates a coating with a bulk uneven filler distribution. Some areas will be rich in particles, while others will be poorer[48-52]. As previously shown, the particle-poorer regions feature

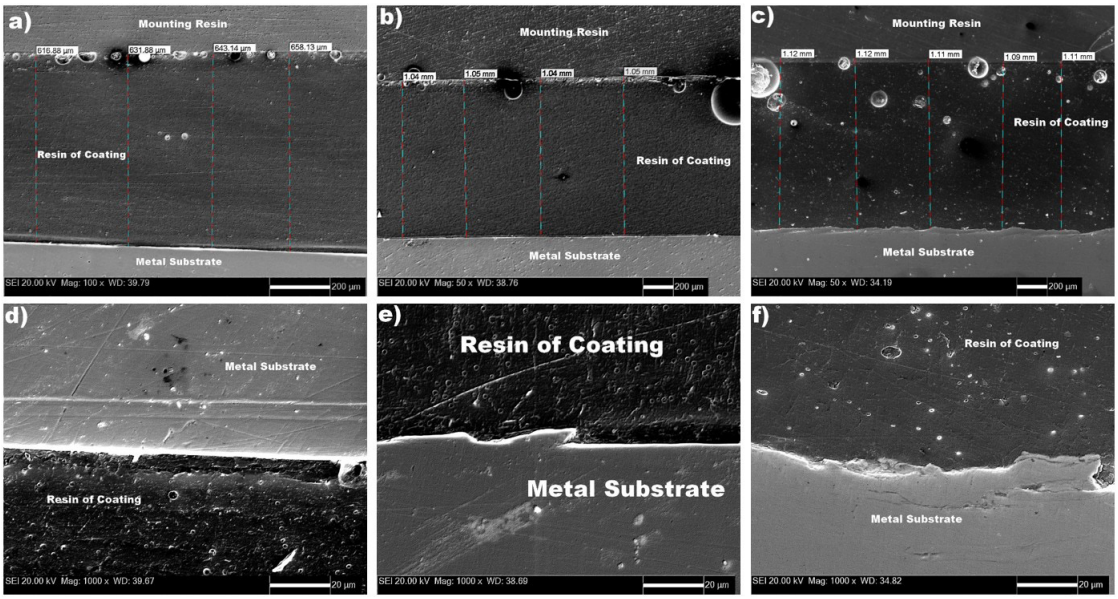

Figure 4. Cross-section SEM images: Thickness measurement: a) COAT, b) COAT0.1OGL and c) COAT0.5OGL and anchoring coating and metallic substrate: d) COAT, e) COAT0.1OGL and f) COAT0.5OGL.

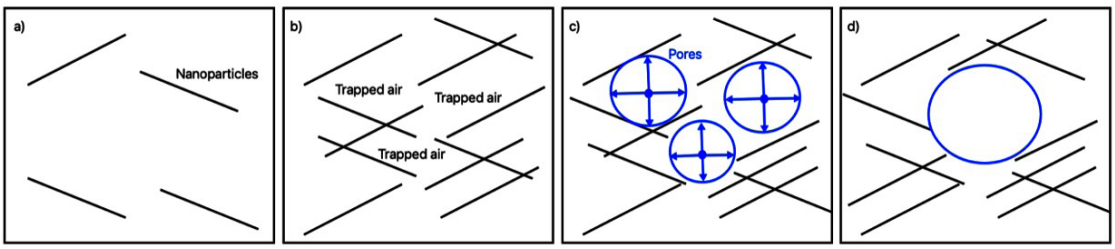

Figure 5. a-c) Scheme showing the interaction between the graphene nanoparticles and trapped air and the development of pores in the resin matrix. c-d) Scheme showing the interaction and segregation between the pores to minimize the system energy, increasing the pores' size and decreasing their volume fraction.

greater crosslinking density. Therefore, the material cure becomes irregular throughout the matrix, promoting shrinkage in areas with great crosslinking density, different from those rich in particles[53]. It was observed (Figure 5) that the increase in the material's particle content increased the pores' size.

The greater the filler content, the more significant the segregation and air-trapped regions within the matrix, causing an increase in the size of pores and a decrease in their volume fraction (Figure 6).

3.2. Coating performance

Shore D hardness measurements were carried out before and after corrosion tests, according to ISO 7619[54], ISO 868[55], ASTM D2240-15[56] and JIS K6253[57] Shore D Durometer equipment (Digimess TH210) was used within the range from 0 to 100, with 0.1 resolution and ±1 accuracy. The coating without the addition of COAT was used as a reference. Table 2 shows the obtained results for all conditions studied. Although the numbers showed minimal variation, it was considered to be within the test uncertainty and taken into account that the graphene addition had no influence on the Shore D hardness.

Table 2. Coating hardness shore D.

Coating	Hardness Shore D	
	Before Corrosion Test	After Corrosion Test
COAT	75.85	77.10
COAT 0.1OGL	72.95	78.10
COAT0.5OGL	78.00	74. 90

Blistering (Figure 7) stands out among the various degradation mechanisms of polymeric films, which consist of forming nodules under the film due to the entrapment of a fluid and/or gas[17,58]. The blistering observed in this study can have its origins in two mechanisms: osmotic blistering, where water-soluble electrolytes, such as chlorides, reaching the metal/coating interface cause corrosion underneath the coating[58], that is, the pressure on the outer side of the coating, being more significant than that on the inner side, accelerates

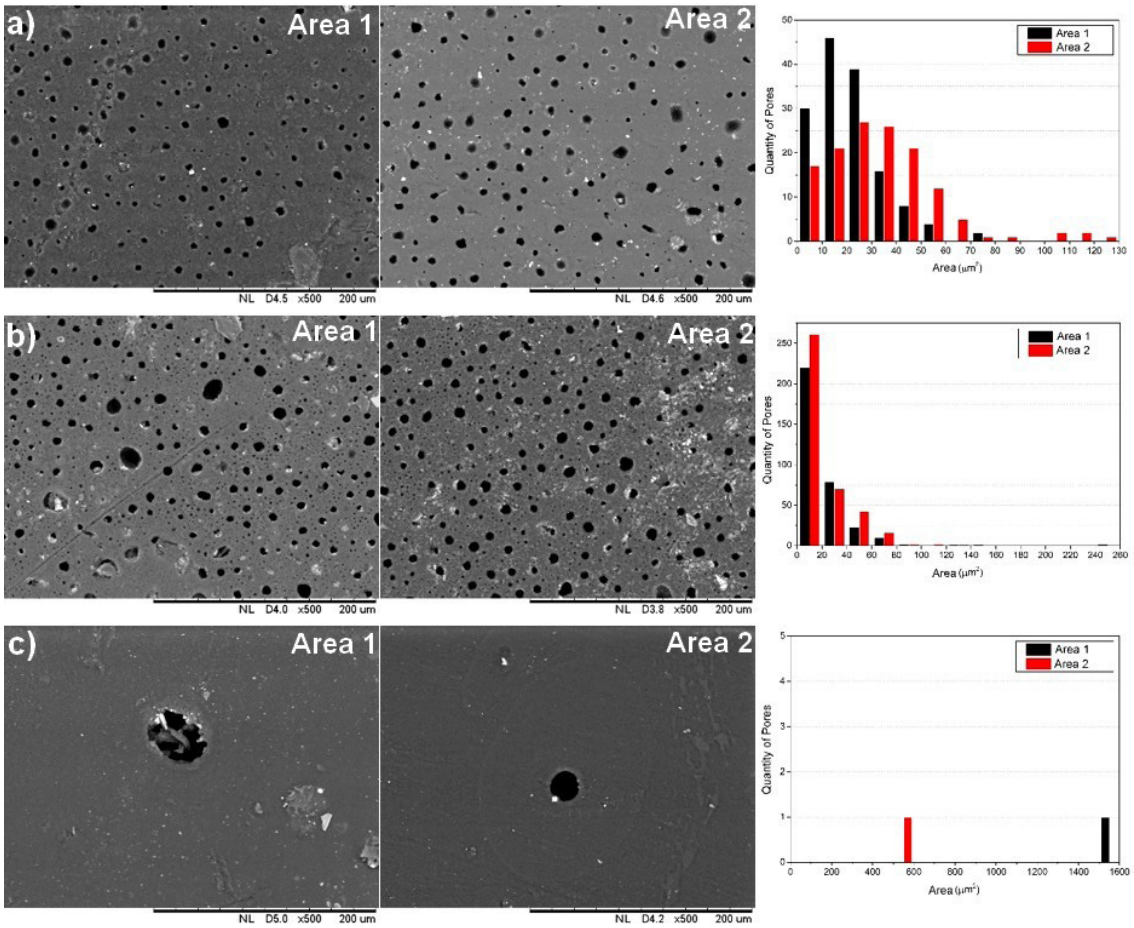

Figure 6. SEM images for porosity density analysis (n^0 of pores x area), considering the comparison of porosity density by area, average pore area and percentage of porous area concerning the total area. Always considering two areas for each condition studied: COAT (a), COAT0.1OGL (b) and COAT0.5OGL (c).

the passage of moisture through the coating film, causing osmotic blistering and thus corrosion. Another probable mechanism could be volume expansion due to swelling. And since organic coatings can absorb $H_2O(g)$, this leads to swelling of the film, which can be localized, thus initiating blistering at the metal/coating interface[58]. The high porosity in COAT and COAT0.1OGL allowed the solution to permeate through the coating for the stipulated test time of 528 h. However, the test time needed to be increased to enable pit formation on the substrate. In the case of COAT0.5OGL, where a significant reduction in porosity was observed, solution permeation was also reduced through the coating, preventing bubbles and blistering regardless of the 70 bar pressure. These results indicate that the studied coating may resist high-pressure and chloride solutions once its porosity density is lowered. After the coatings were removed, reddish spots on the surface of the metallic substrates could be observed, which indicates the presence of iron carbonate (Figure 7c, g, and j, which was easily removed by alcohol.

Graphene addition and distribution will interfere with the mechanical properties of the polymer. As mentioned before, there will be particle-poorer regions with greater crosslinking density. According to the literature[59] and previous tests[35], it can be suggested that these regions are less flexible and, therefore, less susceptible to the percolation of the electrolyte. While the areas with a higher density of particles are more flexible and prone to percolation of the electrolyte[59].

The greater the volume of particles in the system, the longer it takes to oxidize all of them. As the particles oxidize, they also reduce the efficiency of the coating. The bond structure of the resin (polymer) and the graphene system is broken. It is important to point out that although these data were collected under different pressure and temperature conditions, the phenomenon's trend remains the same.

Previous electrochemical evaluations[10] showed that coatings with 0.5 wt.% graphene oxide in the epoxy matrix had inferior performance compared to coatings with 0.1 wt.% in the first hours of the electrochemical evaluation. The sample with a higher volume fraction of graphene oxide (0.5 wt%) showed lower resistivity. However, after an extended period, the sample with 0.1 wt% graphene oxide showed very low resistivity, even less than the sample with pristine epoxy. It was previously demonstrated[35] hat, once particles are better dispersed throughout the matrix in the case of a lower amount of graphene oxide, at first, the coating feature excellent barrier properties and is more evenly spread. But with

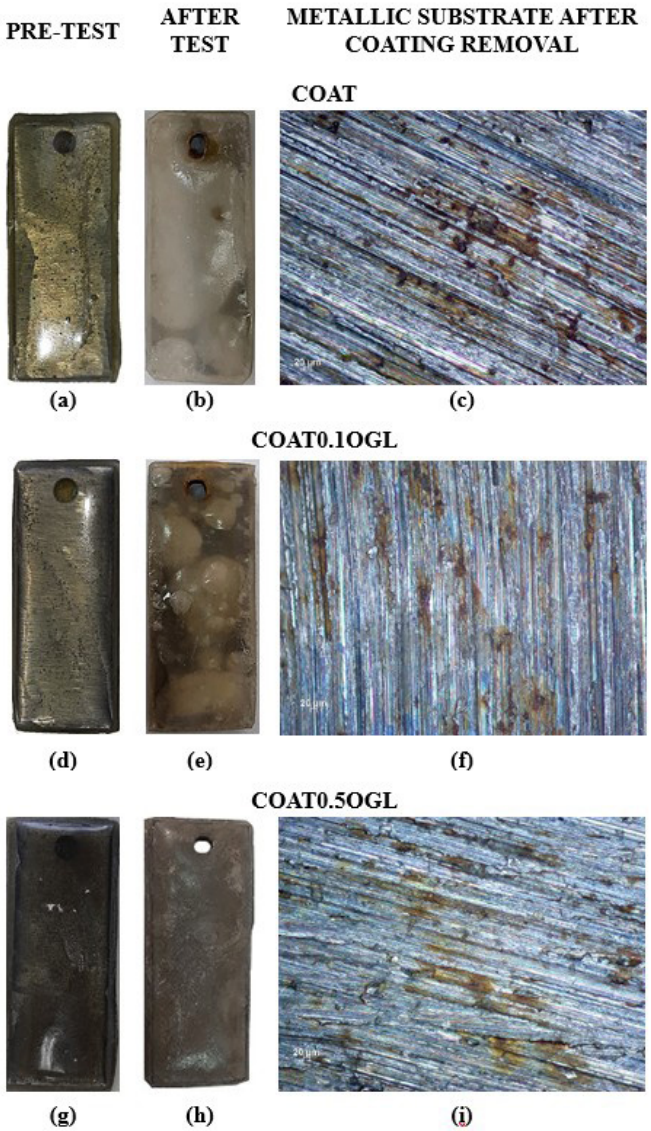

Figure 7. Coupons macro appearance at pre-tests, after test and after coating removal.

extended exposure to the electrolyte, this coating tends to show more significant swelling. The coating with 0.5 wt% has poorer barrier properties initially but withstands long periods of exposure to the electrolyte. The greater amount of non-compatibilized filler within the polymer matrix promotes the formation of clusters, which restrain polymer chain mobility. In the present work, similar behavior has been observed. The sample with a greater amount of graphene oxide showed less porosity (Figure 6), limiting the swelling of the protective coating as seen in the macro image of the samples (Figure 7).

The blistering and porosity observed can have their origins in two mechanisms: osmotic blistering, where water-soluble electrolytes, such as chlorides, reaching the metal/coating interface cause corrosion underneath the coating; that is, the pressure on the outer side of the coating (70 bar), being more significant than that on the inner side, accelerates the passage of moisture through the coating film, causing osmotic blistering and thus corrosion. Another probable mechanism could be volume expansion due to swelling, which depends on time and the graphene density added to the epoxy base coat.

Considering the above mechanisms and the obtained results, the coating with 0.5 wt% initially has poorer barrier properties but withstands long periods of exposure to the electrolyte. In comparison, the coating with 0.1 wt% showed poor performance after lengthy exposure to the electrolyte.

4. Conclusions

The evaluation of the corrosion resistance of an epoxy resin-based coat, reinforced with 0.1 and 0.5 wt% of reduced graphene oxide (rGO), applied to AISI 1020 carbon steel through immersion tests in an aqueous solution with 3.0 wt%

NaCl saturated with CO_2, in a pressurized cell at 70 bar at 40 °C for 528 hours, showed blistering and porosity. Also, the increase in the material's particle content increased the pores' size. The greater the filler amount, the more significant the segregation and air-trapped regions within the matrix, causing an increase in the size of pores and a decrease in their volume fraction.

5. Acknowledgments

The authors wish to thank the Fundação de Amparo à Pesquisa do Estado do Rio de Janeiro (FAPERJ) for Process No E-26/211–744/2015, and Conselho Nacional de Pesquisa CNPq for Project 420912/2018-5. Ananias A. Emmerick thanks CAPES because this study was financed in part by the Coordenação de Aperfeiçoamento de Pessoal de Nível Superior – Brasil (CAPES) – Finance Code 001.

6. References

1. Oliveira JL, Souza W, da Silva CG, Margarit-Mattos ICP, Mattos OR, Quintela JP, et al. Revestimentos anticorrosivos para tanques de armazenamento de petroquímicos. Rev Petr Quim. 2009;319:75-84.
2. Alves BXP, de Moura GL, Galdino TP, Brandão MCR. Estudo comparativo entre os diversos métodos empregados no combate à corrosão na indústria do petróleo. In: Congresso Nacional de Pesquisa e Ensino em Ciências; 2016; Campina Grande. Anais. Campina Grande: Editora Realize; 2016 [cited 2020 Oct 2]. p. 1-10. Available from: https://www.editorarealize.com.br/artigo/visualizar/17994
3. Correa JRP, Souza AM No, Correa ERP. Processo de proteção anticorrosiva aplicado na fabricação de torres eólicas. In: XXXVI Encontro Nacional de Engenharia de Produção - ENEGEP; 2016; João Pessoa. Anais. São José dos Campos: ABEPRO; 2016 [cited 2024 Jan 16]. p. 1-21. Available from: http://www.abepro.org.br/biblioteca/TN_STP_226_321_28896.pdf
4. Zhang SY, Ding YF, Li SJ, Luo X-W, Zhou W-F. Effect of polymeric structure on the corrosion protection of epoxy coatings. Corros Sci. 2002;44(4):861-9. http://doi.org/10.1016/S0010-938X(01)00091-9.
5. Youh MJ, Huang YR, Peng CH, Lin MH, Chen TY, Chen CY, et al. Using graphene-based composite materials to boost anti-corrosion and infrared-stealth performance of epoxy coatings. Nanomaterials (Basel). 2021;11(6):1-21. http://doi.org/10.3390/nano11061603.
6. Kock GH, Brongers MPH, Thompson NG, Virmani YP, Payer JH. Corrosion costs and preventive strategies in the United States [Internet]. Houston: Nace International; 2010 [cited 2020 Oct 23]. 12 p. Available from: http://impact.nace.org/documents/ccsupp.pdf
7. Nunes LP. Fundamentos de resistência à corrosão. Rio de Janeiro: Editora Interciência; 2007. 330 p.
8. Silva MN. Grafeno como nanoaditivo em compósitos para proteção anticorrosiva [dissertation]. Rio de Janeiro: PUC-RJ; 2018.
9. Oliveira AR. Corrosão e tratamento de superfície. Belém: Instituto Federal de Educação, Ciência e Tecnologia; 2012. 104 p.
10. Barbosa MN Jr, Kassab EJ, Quintela JP, Oliveira JL, Batalha JAFL, Falla MPH, et al. Anti-corrosion performance of pigment-free epoxy novolac/reduced graphene oxide composite coatings. Fuller Nanotub Carbon Nanostruct. 2022;30(2):263-74. http://doi.org/10.1080/1536383X.2021.1933956.
11. Petrobras. N-2912 de 08/2011 1ª: Tinta Epóxi " Novolac". Petrobras; 2016.
12. Cui G, Bi ZX, Liu J, Wang S, Li Z. New method for CO2 corrosion resistance Ni-W-Y2O3-ZrO2 nanocomposite coatings. Ceram Int. 2019;45(5):6163-74. http://doi.org/10.1016/j.ceramint.2018.12.093.
13. Camargo PHC, Satyanarayana KG, Wypych F. Nanocomposites: synthesis, structure, properties and new application opportunities. Mater Res. 2009;12(1):1-39. http://doi.org/10.1590/S1516-14392009000100002.
14. DHRA. Tintas anticorrosivas-Informações técnicas [Internet]. São Paulo: DRH-Informações Técnicas; 2024 [cited 2020 Oct 23]. Available from: https://www.tintasanticorrosivas.com.br/informacoes-tecnicas/tintas-anticorrosivas/
15. Perfortex. Perfordur Novolac Tipo II. Rio Claro: Perfortex; 2019. Boletim Técnico.
16. Weg Tintas Ltda. Wegpoxi Block N 2912 Tipo II. Jaraguá do Sul: Weg Tintas Ltda; 2020. Boletim Técnico.
17. Kränke F. Pintura Industrial com Tintas Líquidas. Jaraguá do Sul: Weg Tintas Ltda - DT - 12 Desenvolvimento Tecnológico; 2018.
18. Castro ARP. Impacto da corrosão por CO 2 no Aço AISI 1020 protegido com revestimentos poliméricos [thesis]. Rio de Janeiro: PUC-RJ; 2017.
19. Farag AA. Applications of nanomaterials in corrosion protection coatings and inhibitors. Corros Rev. 2020;38(1):1-20. http://doi.org/10.1515/corrrev-2019-0011.
20. Paiva LB, Morales AR, Díaz FRV. Organophilic clays: characteristics, preparation methods, intercalation compounds and characterization techniques. Ceramica. 2008;54(330):213-26. http://doi.org/10.1590/S0366-69132008000200012.
21. Vianna ES, Rauber MVS, Malfatti CF, Rieder ES. Resistência à corrosão de aço carbono revestido com resina melamina-alquídica contendo nanopartículas de óxido de zinco. Revista de Iniciação Científica da ULBRA. 2012;10:109-12.
22. Madhankumar A, Rajendran N, Nishimura T. Influence of Si nanoparticles on the electrochemical behavior of organic coatings on carbon steel in chloride environment. J Coat Technol Res. 2012;9(5):609-20. http://doi.org/10.1007/s11998-012-9398-6.
23. Madhankumar A, Nagarajan S, Rajendran N, Nishimura T. EIS evaluation of protective performance and surface characterization of epoxy coating with aluminum nanoparticles after wet and dry corrosion test. J Solid State Electrochem. 2012;16(6):2085-93. http://doi.org/10.1007/s10008-011-1623-1.
24. Weg Tintas Ltda. Wegpoxi block n 2912 tipo II. Jaraguá do Sul: Weg Tintas Ltda; 2018. Boletim Técnico.
25. Zhou SQ, Niu YQ, Liu JH, Chen XX, Li CS, Gates WP, et al. Functional montmorillonite/polymer coatings. Clays Clay Miner. 2022;70(2):209-32. http://doi.org/10.1007/s42860-022-00183-8.
26. Rzaij DR, Ahmed NY, Alhboubi N. Coating performance of SiO2/epoxy composites as a corrosion protector. Corros Sci Technol. 2022;21(2):111-20.
27. Xu H, Hu H, Wang H, Li Y, Li Y. Corrosion resistance of graphene/waterborne epoxy composite coatings in CO2-satarated NaCl solution. R Soc Open Sci. 2020;7(5):1-12. http://doi.org/10.1098/rsos.191943.
28. Zhu SD, Li YP, Wang HW, Li JL, Fu AQ, Chen G, et al. Corrosion resistance mechanism of mica–graphene/epoxy composite coating in CO2-Cl− system. Materials (Basel). 2022;15(3):1-17. http://doi.org/10.3390/ma15031194.
29. Sun Y, Wang C, Yuan S, Liang B, Lu R, Li X, et al. Designing multifunctional basalt-CeO2@C3N4/epoxy novolac composite coating with outstanding corrosion resistance and CO2 gas barrier properties. Mater Today Nano. 2024;25:100451. http://doi.org/10.1016/j.mtnano.2024.100451.
30. Hu H, Xu H, Li Y, Cheng X, Li Y. Study of CO2 corrosion behavior of graphene/epoxy composite coating in high chloride environment. Jingbian: Nace International; 2019.
31. Girão DC, Pereira UC, Leite AOS, Araújo WS. Desempenho de revestimentos anticorrosivo epóxi-fosfato de zinco de alta

espessura com adição de argilas montmorilonitas em uma usina Termelétrica a carvão. In: INTERCORR. ABRACO 2018; 2018; São Paulo. Anais. Rio de Janeiro: ABRACO; 2018. p. 1–16.
32. Pourhashem S, Vaezi MR, Rashidi A, Bagherzadeh MR. Exploring corrosion protection properties of solvent based epoxy-graphene oxide nanocomposite coatings on mild steel. Corros Sci. 2017;115:78-92. http://doi.org/10.1016/j.corsci.2016.11.008.
33. Liu D, Zhao WJ, Liu S, Cen QH, Xue QJ. Comparative tribological and corrosion resistance properties of epoxy composite coatings reinforced with functionalized fullerene C60 and graphene. Surf Coat Tech. 2016;286:354-64. http://doi.org/10.1016/j.surfcoat.2015.12.056.
34. Laleh RR, Savaloni H, Abdi F, Abdi Y. Corrosion inhibition enhancement of Al alloy by graphene oxide coating in NaCl solution. Prog Org Coat. 2017;2019(127):300-7. http://doi.org/10.1016/j.porgcoat.2018.11.031.
35. Yuan TH, Zhang ZH, Li J, Zhang DQ, Gao LX, Li WG, et al. Corrosion protection of aluminum alloy by epoxy coatings containing polyaniline modified graphene additives. Mater Corros. 2019;70(7):1298-305. http://doi.org/10.1002/maco.201810549.
36. Yazdi EG, Ghahfarokhia ZS, Bagherzadeh M. Protection of carbon steel corrosion in 3.5% NaCl medium by aryldiazonium grafted graphene coatings. New J Chem. 2017;41(21):12470-80. http://doi.org/10.1039/C7NJ01655G.
37. ASTM International. D4541-17: Standard Test Method for Pull-Off Strength of Coatings Using Portable Adhesion Testers. West Conshohocken, PA: ASTM International; 2017
38. Rajput A, Ak M, Kim SJ, Noh SH, Park JH, Paik JK. Effects of the surface preparation on the life of epoxy coating in steel ship plates: an experimental study. Ships Offshore Struct. 2019;14(Suppl 1):199-206.
39. Ferreira M, Camargo SS Jr, Barbosa BM, Gomes RVB, Lachtermarcher MG, Quintela J. Propriedades mecânicas de epóxis utilizadas no recobrimento interno de oleodutos e gasodutos. Polímeros. 2002;12(3):180-7. http://doi.org/10.1590/S0104-14282002000300010.
40. Weg Tintas e Venizes Ltda. Manual de Manutenção Industrial - Tintas e planos de pintura específicos para a solução anticorrosiva na manutenção industrial [Internet]. Guaramirim: Weg Tintas e Venizes Ltda; 2020 [cited 2020 Oct 23]. 20 p. Available from: https://static.weg.net/medias/downloadcenter/h9c/h19/WEG-tintas-manutencao-industrial-50021433-catalogo-pt.pdf
41. CONTEC: Comissão de Normalização Técnica. Norma-2913-Rev.B: Revestimentos Anticorrosivos para Tanques, Esferas e Cilindros de Armazenamento. Rio de Janeiro: CONTEC - Comissão de Normalização Técnica; 2015.
42. CONTEC: Comissão de Normalização Técnica. Norma-9: Tratamento de Superfícies de Aço com Jato Abrasivo e Hidrojateamento. Rio de Janeiro: CONTEC - Comissão de Normalização Técnica; 2011.
43. Vieira MRS. Avaliação de ensaios simulativos de corrosão e biocorrosão em sistemas estático e dinâmico de revestimentos aplicados em aço carbono [dissertation]. Recife: Universidade Federal de Pernambuco; 2008.
44. Ramanathan T, Abdala AA, Stankovich S, Dikin DA, Herrera-Alonso M, Piner RD, et al. Functionalized graphene sheets for polymer nanocomposites. Nat Nanotechnol. 2008;3(6):327-31. http://doi.org/10.1038/nnano.2008.96.
45. Nawab Y, Shahid S, Boyard N, Jacquemin F. Chemical shrinkage characterization techniques for thermoset resins and associated composites. J Mater Sci. 2013;48(16):5387-409. http://doi.org/10.1007/s10853-013-7333-6.
46. Chen S, Deng Y, Xiao X, Xu S, Rudd PN, Huang J. Preventing lead leakage with built-in resin layers for sustainable perovskite solar cells. Nat Sustain. 2021;4(7):636-43. http://doi.org/10.1038/s41893-021-00701-x.
47. Lorenz N, Müller-Pabel M, Gerritzen J, Müller J, Gröger B, Schneider D, et al. Characterization and modeling cure- and pressure-dependent thermo-mechanical and shrinkage behavior of fast curing epoxy resins. Polym Test. 2022;108:108. http://doi.org/10.1016/j.polymertesting.2022.107498.
48. Bose S, Das A, Basu S, Drzal LT. Covalent functionalization of graphene using polyacryloyl chloride and performance of functionalized graphene–epoxy nanocomposite. Polym Compos. 2018;39(9):3119-28. http://doi.org/10.1002/pc.24318.
49. Orawiec M, Belton D, Telford R, Surtees A. Application of semi-in situ liquid exfoliation of graphite to the scalable production of graphene-epoxy nanocomposites. Polym Compos. 2020;41(11):4933-44. http://doi.org/10.1002/pc.25764.
50. Moeini M, Isfahani RB, Saber-Samandari S, Aghdam MM. Molecular dynamics simulations of the effect of temperature and strain rate on mechanical properties of graphene–epoxy nanocomposites. Mol Simul. 2020;46(6):476-86. http://doi.org/10.1080/08927022.2020.1729983.
51. Szeluga U, Pusz S, Kumanek B, Olszowska K, Kobyliukh A, Trzebicka B. Effect of graphene filler structure on electrical, thermal, mechanical, and fire retardant properties of epoxy-graphene nanocomposites - a review. Crit Rev Solid State Mater Sci. 2021;46(2):152-87. http://doi.org/10.1080/10408436.2019.1708702.
52. Colak OU, Birkan B, Bakbak O, Acar A, Uzunsoy D. Functionalized graphene–epoxy nanocomposites: experimental investigation of viscoelastic and viscoplastic behaviors. Mech Time-Depend Mater. 2023;27(1):185-205. http://doi.org/10.1007/s11043-021-09530-z.
53. Zhao LG, Warrior NA, Long AC. A micromechanical study of residual stress and its effect on transverse failure in polymer-matrix composites. Int J Solids Struct. 2006;43(18-19):5449-67. http://doi.org/10.1016/j.ijsolstr.2005.08.012.
54. ISO: International Organization for Standardization. ISO 7619-1: Rubber, vulcanized or thermoplastic - Determination of indentation hardness - Part 1: Durometer method (Shore hardness). Geneva: ISO; 2006.
55. ISO: International Organization for Standardization. ISO-868-2003: Plastics and ebonite - Determination of indentation hardness by means of a durometer (Shore hardness). Geneva: ISO; 2003.
56. ASTM International. ASTM D2240-15: Standard Test Methods for Rubber Property-Durometer Hardness. In: ASTM International. Annual Book of ASTM Standards [Internet]. West Conshohocken, PA: ASTM International; 2016 [cited 2020 Oct 23]. p. 1-13. Available from: www.astm.org
57. JIS: Japanse Industrial Standard. Standard JIS K6253 (JRMA/JSA) - Rubber, vulcanized or thermoplastic - Determination of hardness. Japan: Japanese Standards Association; 2012.
58. Loghi M. Influência da adição de diferentes oligômeros poliédricos de silsesquioxano (POSS) incorporados na resina epóxi no desempenho à corrosão em substrato de aço de baixa liga [dissertation]. Caxias do Sul: Universidade de Caxias do Sul; 2016.
59. Zimmermann CA, Contri G, Ramôa SDAS, Ecco LG, Barra GMO. The role of the electrical percolation threshold on the anticorrosion performance of an aqueous polyurethane dispersion containing polyaniline. Prog Org Coat. 2022;169:169. http://doi.org/10.1016/j.porgcoat.2022.106921.